Original Article

JCBFM

Journal of Cerebral Blood Flow & Metabolism
2021, Vol. 41(10) 2561–2570

DOI: 10.1177/0271678X211005875
journals.sagepub.com/home/jcbfm
SAGE

Dilated perivascular space is related to reduced free-water in surrounding white matter among healthy adults and elderlies but not in patients with severe cerebral small vessel disease

Yeerfan Jiaerken[1,2], Chunfeng Lian[2], Peiyu Huang[1], Xinfeng Yu[1], Ruiting Zhang[1], Shuyue Wang[1], Hui Hong[1], Xiao Luo[1], Pew-Thian Yap[2], Dinggang Shen[3,4,5,*] and Minming Zhang[1,*]

Abstract

Perivascular space facilitates cerebral interstitial water clearance. However, it is unclear how dilated perivascular space (dPVS) affects the interstitial water of surrounding white matter. We aimed to determine the presence and extent of changes in normal-appearing white matter water components around dPVS in different populations. Twenty healthy elderly subjects and 15 elderly subjects with severe cerebral small vessel disease (CSVD, with lacunar infarction 6 months before the scan) were included in our study. And other 28 healthy adult subjects were enrolled under a different scanning parameter to see if the results are comparable. The normal-appearing white matter around dPVS was categorized into 10 layers (1 mm thickness each) based on their distance to dPVS. We evaluated the mean isotropic-diffusing water volume fraction in each layer. We discovered a significantly reduced free-water content in the layers closely adjacent to the dPVS in the healthy elderlies. however, this reduction around dPVS was weaker in the CSVD subjects. We also discovered an elevated free-water content within dPVS. DPVS played different roles in healthy subjects or CSVD subjects. The reduced water content around dPVS in healthy subjects suggests these MR-visible PVSs are not always related to the stagnation of fluid.

Keywords

Perivascular space, diffusion, free-water, aging, cerebral small vessel disease

Received 2 March 2021; Revised 2 March 2021; Accepted 4 March 2021

Introduction

Perivascular space (PVS) is the fluid-filled compartment around cerebral vessels. It allows exchange between cerebrospinal fluid and interstitial fluid and acts as a conduit for the clearance of certain waste products from the brain.[1] It has been linked to the glymphatic system and is considered to play a vital role in cerebral fluid conduct.[2] Currently, dilated PVS (dPVS) is considered a sign of cerebral small vessel diseases (CSVD). An excessive amount of dPVS is related to cerebral vascular disease and an increased risk of cognitive decline and even dementia.[3–4] However, as higher resolution MR scans were used, dPVS were found in otherwise healthy elderlies or

[1]Department of Radiology, School of Medicine, Second Affiliated Hospital of Zhejiang University, Zhejiang, China
[2]Department of Radiology and BRIC, University of North Carolina at Chapel Hill, Chapel Hill, NC, USA
[3]School of Biomedical Engineering, ShanghaiTech University, Shanghai, China
[4]Shanghai United Imaging Intelligence Co., Ltd, Shanghai, China
[5]Department of Artificial Intelligence, Korea University, Seoul, Republic of Korea

*These authors contributed equally to this work.

Corresponding authors:
Minming Zhang, Department of Radiology, School of Medicine, Second Affiliated Hospital of Zhejiang University, Hangzhou 31000, China.
Email: Zhangminming@zju.edu.cn

Dinggang Shen, School of Biomedical Engineering, ShanghaiTech University, Shanghai, China.
Email: Dinggang.Shen@gmail.com

even younger individuals,[5] it is unclear whether these dPVSs found in different populations have similar pathological or biological significance.

Reduction in fraction anisotropy and increase in mean diffusivity are important and constant findings in CSVD and are related to clinical deficits.[6–7] The prevailing interpretation of these diffusion changes is axon loss and demyelination.[8] However, recent studies showed that increased interstitial water content is the main drive of diffusion parameter changes in CSVD,[9] suggesting dPVS and stagnation of fluid drainage played an important role.[10] However, the presence and extent of changes in normal-appearing white matter water components around dPVS are not clear. Currently, only a few studies explored the change of water content inside PVS by assuming the anisotropic water diffusion within PVS.[10–11] However, no observation was made about how dPVS affects tissue water content around it and how far may this effect spreads, and if there is a distance-related pattern of water content around dPVS.

As such, the purpose of the current study is to explore how dPVS may affect the interstitial water content in and around them, and whether these effects remain the same in subjects of different age groups and conditions. We also tried to discover whether a similar or comparable pattern can be found under a different scanning protocol and voxel size. Since DTI model cannot distinguish different water compartments within and outside axons, and FA and MD are influenced mainly by factors such as fiber orientation and water volume fraction in different compartments. Instead, we employed the NODDI model to separate diffusion signals from interstitial water and intra-axonal water, which exhibits restricted diffusion along the cylindrically shaped axon, providing an opportunity to explore water content changes in different compartments. Furthermore, we developed a method for distance map-based analysis, assigning the distance to the nearest dPVSs surface to each white matter voxel, allowing analysis of the distance-related pattern of different water compartments around dilate PVSs.

Materials and method

Ethics statement

All subjects scanned at Second Affiliated Hospital of Zhejiang University were informed with written consent obtained prior to the study. The study protocol was approved by the human ethics committee of the Second Affiliated Hospital of Zhejiang University, School of Medicine. All clinical investigations had been conducted according to the principle of the Declaration of Helsinki.

Part of the de-identified data was obtained from the HCP-MGH Adult Diffusion Data project, which is an online open-access database. The participants gave written consent, and the procedures were carried out under the institutional review board approval and procedures. The use of the data complied with the HCP Data Use Agreement.

Subjects

This study included subjects from 3 populations, the first two groups were of the same scanning protocol, and the third group was from HCP-MGH Adult Diffusion Database with a different scanning protocol to ensure that our discovered patterns are not parameter-specific and are comparable under different parameters.

The first group of subjects was collected from the Department of Neurology, Second Affiliated Hospital of Zhejiang University, School of Medicine (referred to as the "CSVD group"). Patients diagnosed with lacunar infarction from at least 6 months before the scan were provided with an opportunity to participate in this study. Fifteen patients were retrospectively included. The inclusion criteria are: (1) with visible dPVS on T2 weighted image; (2) agreed to participate and without the exclusion criteria: (1) MR incompatible; (2) excessive WMH ($>=25\%$ of total white matter volume) that would cause difficulties in PVS segmentation; (3) history of stroke (except lacunar infarction), multiple sclerosis, Alzheimer's disease, Parkinson's disease, and head trauma; (4) low image quality such as head motion and other artifacts.

The Second group (referred to as the "Healthy aging group") was healthy age-matched volunteers recruited from nearby communities. Twenty subjects were enrolled based on the inclusion criteria of (1) age $>$ 55-year-old; (2) with visible dPVS on T2 weighted image; (3) agreed to participate and without the exclusion criteria: (1) MR incompatible; (2) history of other cerebral small vessel diseases including WMH, lacunar infarction, and microbleed; (3) history of stroke, multiple sclerosis, Alzheimer's disease, Parkinson's disease, and head trauma; (4) low image quality such as head motion and other artifacts.

The third group was 35 healthy subjects aged from 20$\sim$59 from the HCP-MGH Adult Diffusion Data project (Hereafter referred to as the "Healthy adult group"). The data is available to those who register and agree to the Open Access Data Use Terms. Image data were downloaded and examined. Subjects with complete T1, T2, and diffusion images were included in our study. After inspection, three subjects were removed due to a lack of T2 image. Another 4

subjects were removed due to head motion and visible artifact on the image (Figure 1).

MRI protocol

All subjects from the CSVD group and the Healthy aging group were scanned at Second Affiliated Hospital of Zhejiang University, School of Medicine using a 3 T MR (MR750 GE healthcare, Unite States) scanner with an 8-channel brain phased array coil. Patients were instructed to not move their heads, and foam paddings were used to restrict head motion. Upon detection of obvious head motion during scanning, the affected sequence would be discarded and rescanned. Scanning protocols are: (1) High resolution 3 D sagittal T1-weighted imaging (T1WI) was acquired using spoiled gradient echo sequence with TR/TE = 7.3/3.0 ms, TI = 450 ms, flip angle = 8°, slice

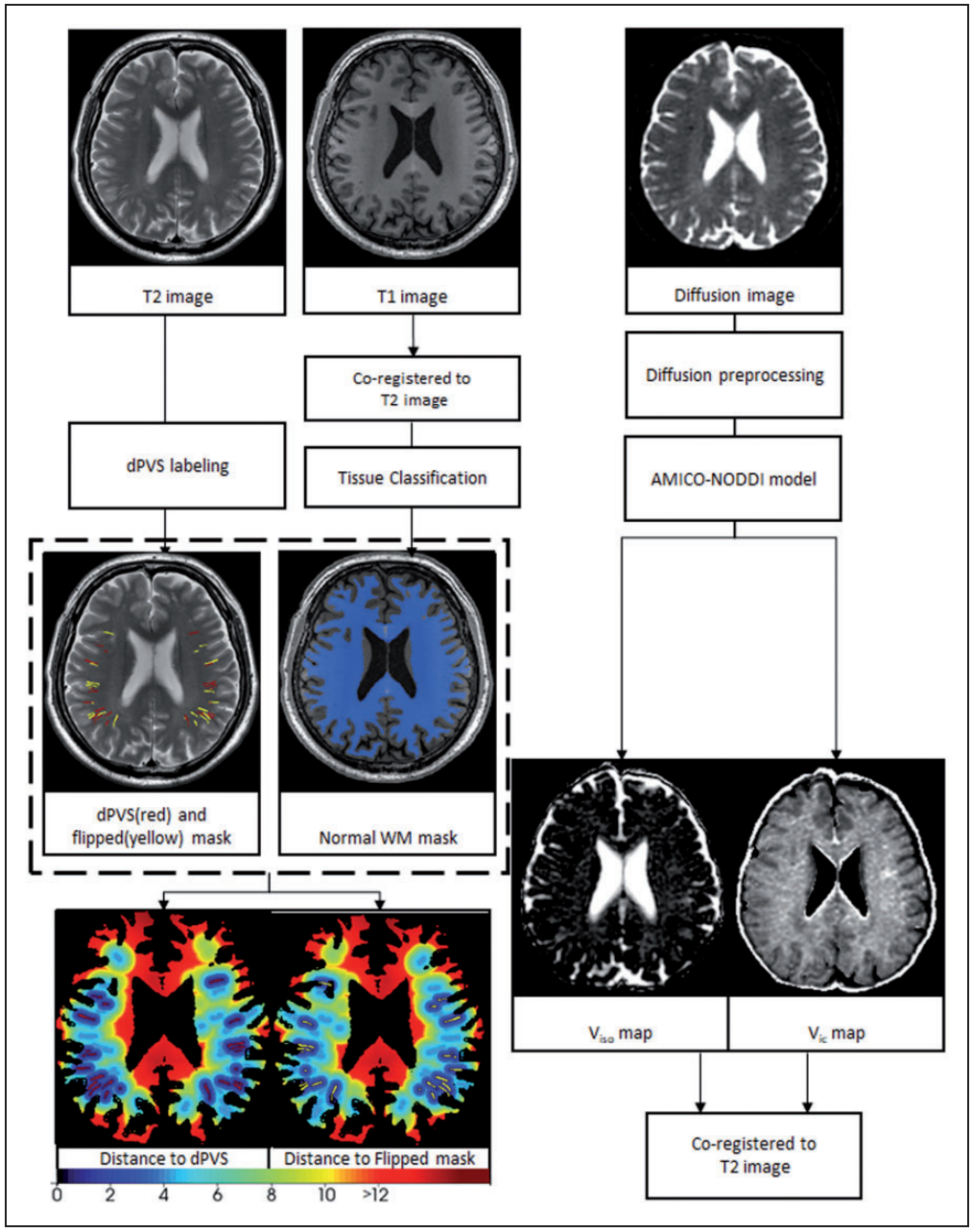

Figure 1. T2 images were used to create the dilated perivascular space (dPVS) masks. Then random lineal structures were generated at nearby white matter (phantom dPVS). The overlapped PVS voxels were removed from the phantom dPVS. Then for each voxel on the normal white matter mask, 2 distance values were calculated: the distance to the nearest dPVS and the distance to the nearest phantom dPVS. The respective distance maps were generated by assigning the distance value to each voxel.

thickness = 1 mm, matrix = 250 × 250, FOV = 25 cm. (2) T2WI TR/TE = 3000/106.8, voxel size = 1*1*4. (3) T2 FLAIR: TR/TE = 8400/152 ms, TI = 2100 ms, flip angle = 90°, slice thickness = 4 mm without slice gap, matrix size = 256 × 256, FOV = 24 cm). (4) Diffusion scan was acquired using a single-shot, spin–echo planar imaging (EPI) sequence with TR/TE = 5000/95 ms; slice thickness = 2 mm without slice gap; FOV: 256 mm × 256 mm; matrix: 128 × 128; and three diffusion weighting (b) values (0, 1000, and 2000 s/mm^2), with diffusion encoding in 30 directions for every b-value.

The subjects from the HCP-MGH Adult Diffusion Data project received their scanning on the customized Siemens 3 T Connectom scanner, which is a modified 3 T Skyra system (MAGNETOM Skyra Siemens Healthcare), housed at the MGH/HST Athinoula A. Martinos Center for Biomedical Imaging (see refernce[12] for details of the scanner design and implementation). A 64-channel, tight-fitting brain array coil[13] was used for data acquisition. The imaging protocols are: (1) T1-weighted imaging scan was acquired with TR/TE = 2530/1.15 ms, TI = 1100 ms, flip angle = 7°, 1 mm isotropic, FOV = 256*256. (2) T2 weighted image, TR/TE = 3200/561 ms, 0.7 mm isotropic, FOV = 224*224. (3) Diffusion scans were acquired using spin-echo EPI sequence with TR/TE = 8800/57, δ/Δ = 12.9/21.8, FOV = 210*210, Matrix = 140*140, 1.5 mm isotropic, Multiband factor = 1, Echo spacing = 0.63(ms), b-values = 1000, 3000, 5000, 10000 s/mm^2. Due to the fact that NODDI assumes gaussian diffusivity across compartments. However this assumption is drastically violated at high b-values, we removed the b = 5000 and b = 10,000 images, using only the b = 0, 1000, and 3000 images to reconstruct the NODDI parameters.

Image analysis

PVS labeling. DPVSs on the 3 D T2 images from the HCP-MGH database were automatically segmented. PVS segmentations were obtained using a multi-channel multi-scale fully convolutional network developed and explained in detail in our previous work.[14] Briefly, the original T2-weighted images were first enhanced via a non-local Haar-transform-based line singularity representation method. Then both the original and enhanced MR images were used as multi-channel input, and multi-scale features were automatically learned to distinguish the PVSs and surrounding brain tissue. After the automatic segmentation, the PVS masks were manually checked and corrected by an experienced radiologist (Y.J.) (Figure1, Supplementary Figure 1). Due to the algorithm was developed for 3 D images and the performance was not optimal for 2 D images, the 2 D images scanned at Second Affiliated Hospital of Zhejiang University School of Medicine were manually labeled by an experienced radiologist and reviewed by two other experienced radiologists. A Consensus was reached through discussion over dispersion.

"Phantom dPVS". However, we are aware that dPVS tend to appear in specific white matter areas of the brain (in areas closer to the cortical gray matter). This tendency of appearing in a specific white matter area could contaminant our results because different white matter areas could have intrinsic differences in nonparenchymal water fractions. To make sure the distance-related pattern of nonparenchymal water fractions are specific to dPVS and not due to the intrinsic difference between different white matter regions, a number of voxels in normal-appearing white matter region where dPVS often appear were selected. These non-PVS control voxels were selected by flipping and reorienting the current dPVS mask, resulting in a "phantom dPVS" mask. Then the original PVS mask was subtracted from the phantom mask to make sure no "real" dPVS were included in the phantom masks. This way, we accounted for the intrinsic differences caused by different white matter regions.

Obtaining the normal white matter mask. T1 and T2FLAIR images were co-registered to the T2 image of the same subjects. Then T1 images were used to create the white matter mask with the segmentation tool of SPM 12. T2FLAIR images were used for WMH segmentation with the Lesion Segmentation Tool of SPM 12. The WMH labeling steps were not conducted on subjects from the HCP-MGH data set as they are young and healthy with little WMH, and T2 FLAIR images were not available for them. Normal-appearing white matter masks were obtained by subtracting WMH masks from the white matter mask, whereas in the HCP-MGH data set, the segmented WM masks are considered to be the normal-appearing white matter masks (Figure 1).

Distance mapping. After obtaining the normal-appearing white matter masks and PVS masks, for each voxel in the normal-appearing white matter mask (i_1, i_2, i_3...i_n), the pairwise Euclidean distances between the given voxel i_x and every voxel on the PVS mask (j_1, j_2, j_3 ... j_m) were calculated, and the smallest distance among them is the distance for the voxel i_x to the nearest PVS (denoted by d_{pvs}). And for each voxel on the normal-appearing white matter mask, its intensity is set to this distance. Similarly, another set of distance maps was obtained by calculating and assigning the distance between each white matter voxel to the nearest phantom mask (denoted by $d_{control}$) (Figure 1). The voxels

were then categorized into 10 layers with thicknesses of 1 mm based on their distance to the nearest dPVS surface (determined by the d_{pvs} value), resulting in a layered normal-appearing white matter mask. And then the process was repeated for each voxel based on their $d_{control}$ value (Figure 2).

Preprocessing of multi-shell diffusion data. Raw diffusion data from the 2nd affiliated hospital of Zhejiang University were motion-corrected, and eddy current corrected using Freesurfer and FSL, respectively.

HCP MGH diffusion data underwent motion and eddy current correction before downloaded. The $b = 0$ images interspersed throughout the diffusion scans were used to estimate the bulk head motions based on the initial time point (first $b = 0$ image), where a rigid transformation was calculated with the boundary-based registration tool in the FreeSurfer package V5.3.0. For each $b = 0$ image, this transformation was then applied to itself, and the following 13 diffusion weighted images to correct for head motions. After motion correction, the b-vectors were adjusted according to the rigid rotation estimated.

NODDI model fitting. The NODDI model[15] separated cerebral water into 3 main compartments: 1) Intracellular volume, which is water diffusing in a "cylindrical" motion along a long tube-like structure, like in myelinated axon. 2) The extra-cellular volume where water motion is hindered but not restricted, like in extra-cellular space. 3) Isotropic volume refers to water moving in isotropic motion, like in cerebral spinal fluid. The Python-based AMICO-NODDI software[16] was used to fit the preprocessed multi-shell diffusion data, and 2 parameter maps (isotropic volume fraction, V_{iso} and intra-cellular volume fraction, V_{ic}) were obtained based on the equation (1) and (2).

$$(1 - V_{iso})\ (V_{ic} + V_{exc}) + V_{iso} \quad (1)$$

$$V_{ic} + V_{exc} = 1 \quad (2)$$

Parameter reading and statistical analysis. The mean V_{ic} and V_{iso} were calculated for all voxels in each layer around dPVS and phantom dPVS (Figure 2). To test if there were significant differences in the V_{ic} and V_{iso} between voxels around the dPVS and phantom dPVS, for each category, pairwise t-tests were conducted between the mean V_{ic} and V_{iso}, e.g. the mean V_{iso} in the first layer around dPVS is compared with the mean V_{iso} in the first layer around phantom dPVS, and so forth. Because there were 10 layers and 3 groups, and the pairwise t-tests were conducted 60 times. Bonferroni corrections were used, and the P value of significant difference was set to $0.05/60 \approx 0.00083$. A Repeated measures analysis of variance (RANOVA) was used to test if there are significant Viso changes in each layer, and to test the impact of age, scanner, and CSVD status on Viso. Model have Viso in different layers as the responses and scanner, age and CSVD statues as the predictors. To further compare if there were group differences in the Viso in dPVS, The Viso of dPVS between different groups were compared using the ANOVA test. Further Pearson correlation tests were conducted within each group to test if the Viso in dPVS is correlated with the Viso of the whole-brain normal-appearing white matter. Data was tested with Lilliefors test for normality.

Results

From the original 35 HCP-MGH subjects, 3 were removed due to lack of T2 image, and 4 were removed

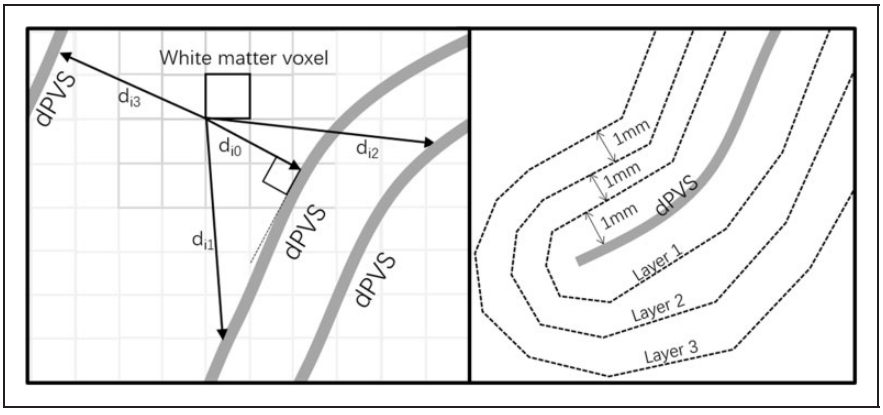

Figure 2. For a specific white matter voxel, it has a distance value to each dPVS voxel (d_{i0}, d_{i1}, d_{i2}...). And within all these distance values, the d_{i0} is the smallest for it is perpendicular to the nearest dPVS. The voxels were categorized into 10 layers with 1 mm thickness based on their distance to the nearest dPVS surface, resulting in a layered normal-appearing white matter mask.

due to head motion and visible artifact. Demographic data were provided in Table 1.

The mean V_{ic} and V_{iso} at each distance-associated category for each group were plotted in Figure 3(a) to (f), as well as an illustrative figure was provided in Figure 3(g). In all 3 groups, the V_{ic} around dPVS did not differ from that of the phantom dPVS (Pair-wise t-test P values >0.05 at all distance ranges). However, V_{iso} from $0\sim1$mm and $1\sim2$mm around dPVS is significantly higher than that of control points in all groups. And V_{iso} from $2\sim4$mm from dPVS is significantly lower than that of control points in the healthy elderly group, and And Viso from $3\sim6$ mm from dPVS is significantly lower than that of control points in the healthy adult group. In the CSVD group, the Viso is lower only at $3\sim4$mm from dPVS than control points, and the differences were smaller than the rest of the groups. Because our diffusion data from the Second Affiliated Hospital of Zhejiang University have a voxel size of 2 mm, a separate analysis with 5 layers with 2 mm thick was conducted and the result can be found in Supplementary Figure 2.

RANOVA results showed that layered distance (reflect by the intercept) and CSVD have a significant impact on Viso (Table 2). ANOVA analysis results suggest that there are significant differences in V_{iso} within 2 mm from the dPVS between the 3 groups ($P<0.001$). Further post-hoc analysis using LSD correction revealed that the differences were significant between each pair of the 3 groups (Figure 4). The CSVD group had the highest V_{iso} within dPVS, while the healthy adult group had the lowest. The Pearson correlation test between V in dPVS and the V across the entire normal-appearing white matter showed a significant positive correlation in the Healthy Elderly group and the Healthy Adult group ($P<0.001$), but not in the CSVD group ($P=0.888$) (Figure 5).

Discussions

In the present study, we analyzed the pattern of distance-related nonparenchymal water content distribution around dPVS, and we examined this pattern in 3 groups of subjects from different populations. We discovered that there were increased isotropic water volume fraction in voxels contain or partially contain dPVS ($0\sim2$mm around dPVS segmentation), and that there were decreased isotropic water volume fraction in voxels $2\sim6$mm around PVS in the healthy subjects. Whereas in the subjects with extensive CSVD, the increased isotropic water volume fraction in dPVS become more prominent, and the decrease of isotropic water volume fraction around dPVS becomes less significant. This pattern was validated across different voxel-size and diffusion protocols, suggesting the robustness of the results.

The discovery of increased V_{iso} at $0\sim2$mm around dPVSs is most likely to be driven by the water signal inside the dPVSs, especially considering our images have a spatial resolution of 1.5 mm for the HCP-MGH dataset and 2 mm for the rest data sets. A previous study suggested that PVS has an anisotropic diffusion since it has a tubular structure and directional water movement, it is also possible to be isotropic under certain condition,[10] e.g. when the PVS is dilated enough that the diameter of the PVS is larger than the water can diffuse during the diffusion time, and hile the directional motion in the PVS is slow enough, then the water diffusion could appear isotropic.[10] Also, there were no differences in the V_{ic} compartment around dPVS, which reflected no significant change in the volume distribution of the non-isotropic diffusion compartment, this further suggests that water in dPVS could exhibit an isotropic diffusion.

The most noteworthy finding is that V_{iso} in healthy adults and healthy elderly subjects are decreased in areas from $2\sim6$mm around dPVS when compared to normal-appearing white matter areas. This finding

Table 1. The demographic data of subjects in different groups.

Characteristics	CSVD group	Healthy elderly	Healthy adult
Number of subjects	15	20	28
Age, mean (range), year	67.1 (57 ~ 81)	63.6 (56 ~ 83)	31.9 (20 ~ 59)[a]
Women	4	15	13
Education, mean (range), year	7.1 (3 ~ 12)	9 (4 ~ 16)	NA[b]
MMSE score, mean (range)	26.8 (25 ~ 29)	27.3 (24 ~ 30)	NA[b]
Cardiovascular risk factors or diseases			
Current smoker	1	1	NA[b]
Type 2 diabetes	0	0	NA[b]
Hypertension	4	1	NA[b]

[a]The HCP-MGH database only provided a age range for each de-identified subject not the specific age.
[b]HCP-MGH adult diffusion data set did not provide detailed demographic data, but reported the subjects were healthy at enrollment.

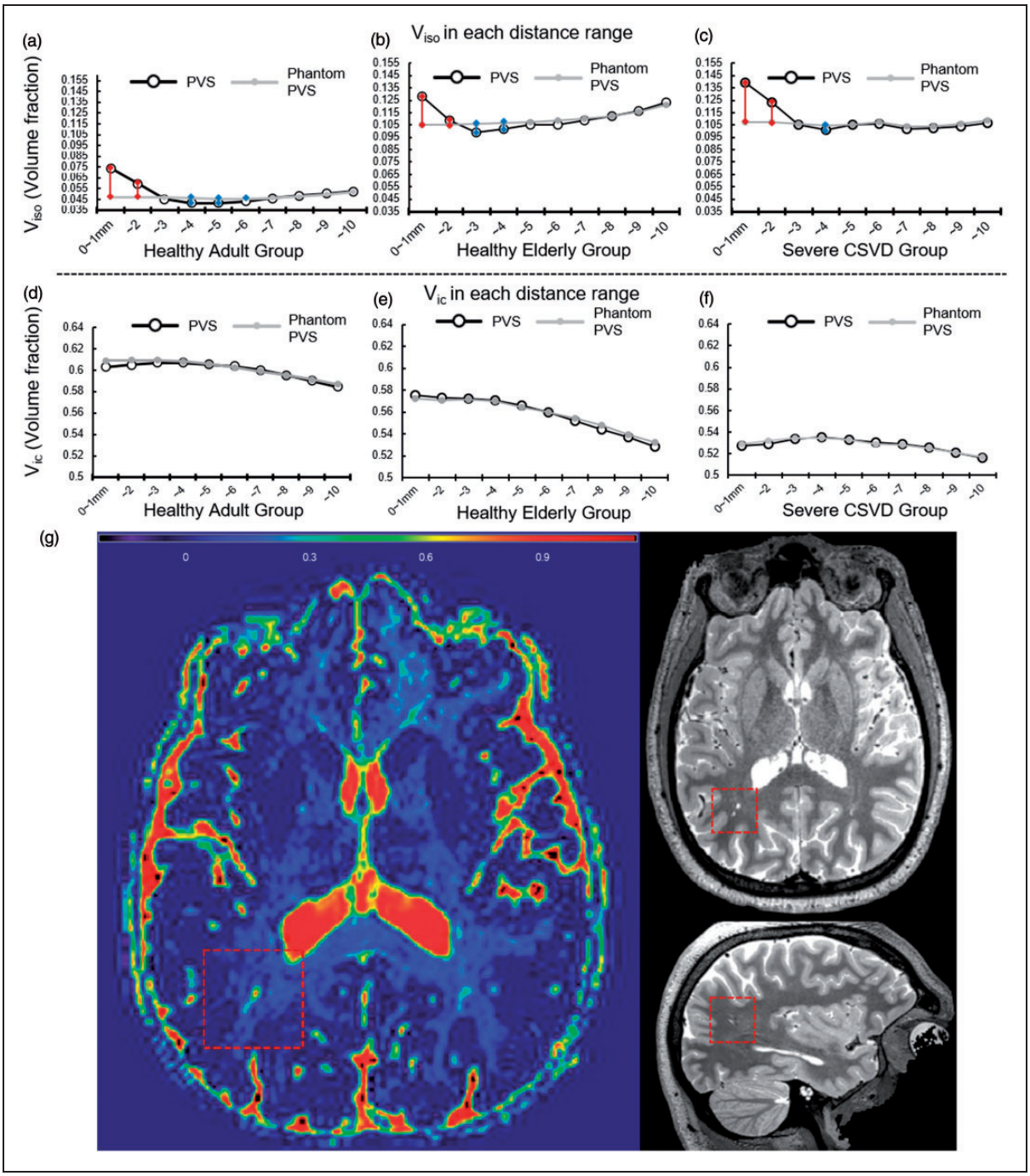

Figure 3. (a–f) The volume fraction of isotropic water compartment (V_{iso}, %) and Volume fraction of intra-cellular water compartment (V_{ic}, %) in each layer. Horizontal axes are the distance to the nearest dilated perivascular space (dPVS) or phantom dPVS. Vertical axes are the mean V_{iso} (or V_{ic}) in that layer. Red lines denote V_{iso} is significantly higher around the dPVS than around the phantom in that specific layer between the connected pair, and blue line vice versa. P values were adjusted due to multiple comparisons using the Bonferroni method: $P < 0.00083$. G: Illustrative figure showing a large PVS in a healthy adult (27 y-o). Viso map showed significantly increased signal intensity. A relatively lower signal intensity area surrounding the large PVS can be noted.

somewhat contradicts the previous belief that the dPVS is related to increased water content around it. This decrease much weaker in subjects with extensive CSVD. One possible explanation is these dPVSs or "MR-visible" PVSs in healthy subjects could accelerate the draining of interstitial fluid around it, thus reducing the water content. Though there is currently no direct evidence to prove the dPVSs could accelerate fluid

Table 2. The repeated measures analysis of variance results.

Responses: Viso in different distance (Layers)				
	SumSq	MeanSq	F	p*
Intercept (Distance)	0.0028	0.00031	4.98	0.012**
Scanner:	0.0011	0.00015	2.02	0.14
CSVD	0.0046	0.00051	8.19	0.00096**
Age	0.0011	0.00012	1.94	0.16
Error	0.027	6.25E-05		
Repeated measures analysis of variance (RANOVA)				

*Greenhouse-Geisser corrected
**Corrected $P < 0.05$

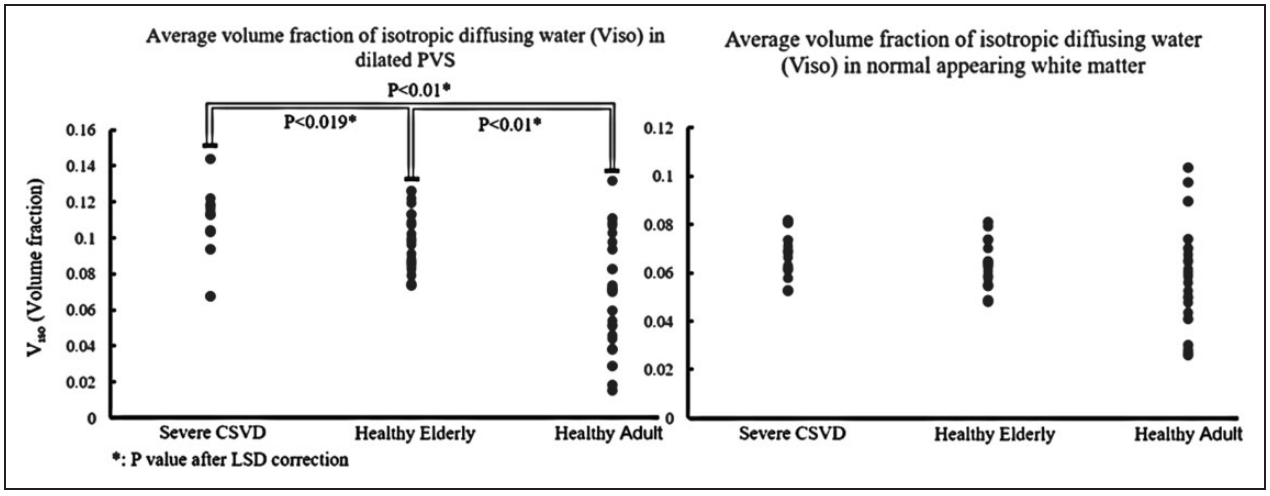

Figure 4. (a) Dotted plot showing the differences of the Volume fraction of isotropic water compartment (V_{iso}, %) within dilated perivascular space (dPVS) between different groups, CSVD group had the highest V_{iso}. (b) the differences of V_{iso} across the entire normal white matter between the three groups. There was a trend of CSVD group having the highest V_{iso} and healthy adults having the lowest V_{iso} but didn't reach statistical significance (ANOVA $P = 0.241$).

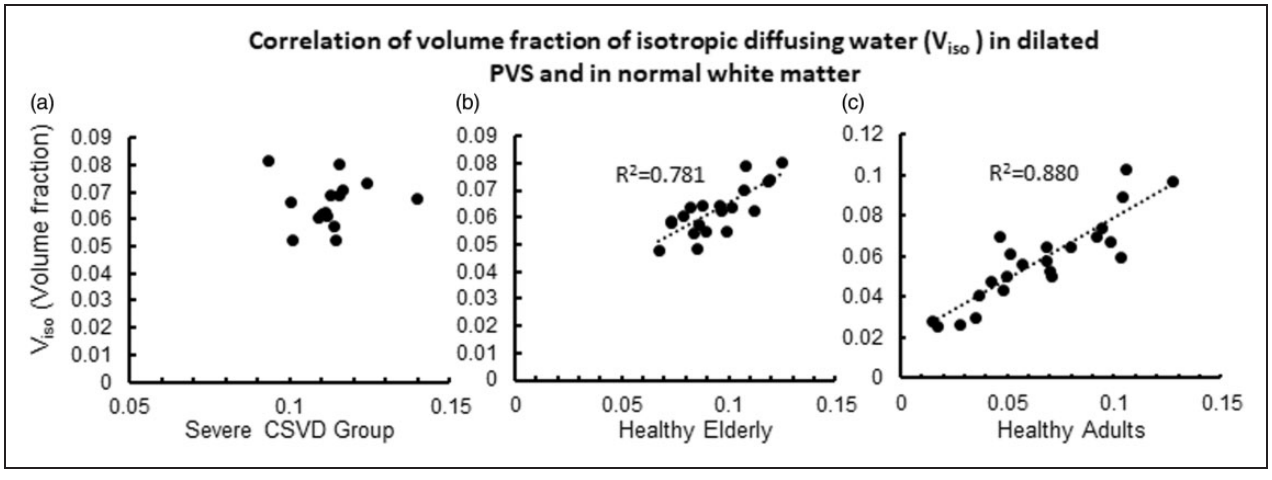

Figure 5. The Correlation between V_{iso} (volume %) in dPVS and normal white matter. The correlation was not significant in the CSVD group. The horizontal axes represent the V_{iso} in dPVS and the vertical axes represent the V_{iso} in normal white matter.

drainage, a study observed diurnal fluctuation of diffusion signal [17] caused by changes in the perivascular pathway, and another study also find the activity of PVS is different under anesthetics or waken states.[2] This evidence supported the possibility of PVS dilating or closing to adjust fluid drainage. After ischemic stroke, an increased number of PVS in the lesion is related to better recovery and accelerated metabolism of waste products.[18] These studies suggest that PVS has the potential to dilate and accelerate waster clearance. On the other hand, in elderly subjects with CSVD, the decrease of V_{iso} around dPVS is much weaker, which could be explained by the stagnation of fluid drainage and the failure of compensation, which limited further acceleration of fluid clearance. This is further supported by a previous study on WMH formation around dPVS in CSVD patients.[19]

It should also be noted that the dPVS in the CSVD group showed higher V_{iso} than in healthy subjects, and the healthy elderly had higher V_{iso} than healthy adults. Higher V_{iso} reflects a higher volume fraction of isotropic water fraction in the voxel containing dPVS, which could be interpreted as an increased partial volume fraction of dPVS in a voxel, which means larger PVS. And larger dPVS in CSVD is in par with the previous observation of more severe dPVS in the CSVD.[20] More supportive evidence comes from studies from Bouvy et al.[21] and Goodman et al.,[22] whose studies demonstrated small vessel angiopathy and disrupted vasomotor function, both considered pathologies related to CSVD, are closely related to dPVS. On the other hand, the V_{iso} changes in the dPVS of healthy subjects are highly correlated with the global white matter V_{iso}, which could be interpreted as a mechanism of maintaining fluid balance. While in the CSVD subject, the V_{iso} in dPVS and global white matter are no longer correlated in our study, supporting the hypothesis of dysfunctional PVS in CSVD subjects and that CSVD is a wide-spreading condition that can affect the whole brain instead of just restricted to the focal lesion. However, as currently the exact mechanism of water transport within PVS is still being debated,[23–24] any interpretation of water diffusion results should be made with caution. Nevertheless, our result suggested that dPVS found in healthy young subjects and elderly subjects with CSVD could reflect different physiological or pathological processes and that dPVS could be a heterogenetic entity, which could help to explain the uncertainty in the clinical correlation of dPVS in previous studies.

Limitations

Because PVS are small and thin linear structures on T2 image, the slightest movement could cause misalignment of PVS and related diffusion map. Care was taken to ensure the best image quality in our study, but future studies with dedicated scanning protocol and deep learning base co-registration technique can analyze the imaging of PVS more accurately. Secondly, NODDI assumes a fixed diffusivity during fitting, which could be violated in the presence of pathology. So part of the change in the Viso could be the result of a change in tissue diffusivity instead of an actual change in water content. Future pathological studies and studies using techniques like diffusion spectrum imaging that do not assume a fixed diffusivity could be better equipped to explore the varies.

Summary

DPVS could reflect different physiological or pathological processes in healthy young and elderly subjects with CSVD. DPVS in younger healthy subjects is not necessarily related to pathological changes.

Funding

The author(s) disclosed receipt of the following financial support for the research, authorship, and/or publication of this article: This study was funded by the 13th Five-year Plan for National Key Research and Development Program of China (Grant No. 2016YFC1306600), Zhejiang Provincial Natural Science Foundation of China (grant number: LSZ19H180001), National Natural Science Foundation of China (grant number: 81271530 & 81771820 & 81901706) and Health and Family Planning Commission of Zhejiang Province(grant number: 2016KYA099). Part of the data used in the preparation of this work was obtained from the Human Connectome Project (HCP) database (https://ida.loni.usc.edu/login.jsp). The HCP project (Principal Investigators: Bruce Rosen, M.D., Ph.D., Martinos Center at Massachusetts General Hospital; Arthur W. Toga, Ph.D., University of Southern California, Van J. Weeden, MD, Martinos Center at Massachusetts General Hospital) is supported by the National Institute of Dental and Craniofacial Research (NIDCR), the National Institute of Mental Health (NIMH) and the National Institute of Neurological Disorders and Stroke (NINDS). HCP is the result of efforts of co-investigators from the University of Southern California, Martinos Center for Biomedical Imaging at Massachusetts General Hospital (MGH), Washington University, and the University of Minnesota.

Declaration of conflicting interests

The author(s) declared no potential conflicts of interest with respect to the research, authorship, and/or publication of this article.

Authors' contributions

Y.J.: conception and design of the study, analysis of data, drafting the manuscript and figures.
CF.L.: analysis of data.
PY.H.: conception and design of the study, analysis of data.

XF.Y.: conception and design of the study.
RT.Z.: conception and design of the study.
SY.W.: conception and design of the study, data acquisition.
H.H.: conception and design of the study, data acquisition.
X.L.: conception and design of the study.
PT.Y.: drafting the manuscript.
DG.S.: drafting the manuscript.
MM.Z.: conception and design of the study, drafting the manuscript.

Availability of data and materials

Data used in this manuscript from HCP-MGH database are publicly available in the HCP-MGH database repository, at http://protocols.humanconnectome.org/. The datasets form Second Affiliated Hospital of Zhejiang University used and analyzed during the current study are available from the corresponding author on reasonable request.

Supplementary material

Supplemental material for this article is available online.

References

1. Rasmussen MK, Mestre H and Nedergaard M. The glymphatic pathway in neurological disorders. *Lancet Neurol* 2018; 17: 1016–1024.
2. Bechet NB, Kylkilahti TM, Mattsson B, et al. Light sheet fluorescence microscopy of optically cleared brains for studying the glymphatic system. *J Cereb Blood Flow Metab* 2020; 40: 1975–1986.
3. Wardlaw JM, Smith Ee Biessels GJ, et al. Neuroimaging standards for research into small vessel disease and its contribution to ageing and neurodegeneration. *Lancet Neurol* 2013; 12: 822–838.
4. Zhu YC, Dufouil C, Soumare A, et al. High degree of dilated Virchow-Robin spaces on MRI is associated with increased risk of dementia. *J Alzheimers Dis* 2010; 22: 663–672.
5. Zhu YC, Dufouil C, Mazoyer B, et al. Frequency and location of dilated Virchow-Robin spaces in elderly people: a population-based 3D MR imaging study. *AJNR Am J Neuroradiol* 2011; 32: 709–713.
6. Promjunyakul NO, Lahna DL, Kaye JA, et al. Comparison of cerebral blood flow and structural penumbras in relation to white matter hyperintensities: a multi-modal magnetic resonance imaging study. *J Cereb Blood Flow Metab* 2016; 36: 1528–1536.
7. Jiaerken Y, Luo X, Yu X, et al. Microstructural and metabolic changes in the longitudinal progression of white matter hyperintensities. *J Cereb Blood Flow Metab* 2019; 39: 1613–1622.
8. Murray ME, Vemuri P, Preboske GM, et al. A quantitative postmortem MRI design sensitive to white matter hyperintensity differences and their relationship with underlying pathology. *J Neuropathol Exp Neurol* 2012; 71: 1113–1122.
9. Sepehrband F, Cabeen RP, Barisano G, et al. Nonparenchymal fluid is the source of increased mean diffusivity in preclinical Alzheimer's disease. *Alzheimers Dement* 2019; 11: 348–354.
10. Sepehrband F, Cabeen RP, Choupan J, et al. Perivascular space fluid contributes to diffusion tensor imaging changes in white matter. *Neuroimage* 2019; 197: 243–254.
11. Taoka T, Masutani Y, Kawai H, et al. Evaluation of glymphatic system activity with the diffusion MR technique: diffusion tensor image analysis along the perivascular space (DTI-ALPS) in Alzheimer's disease cases. *Jpn J Radiol* 2017; 35: 172–178.
12. Setsompop K, Kimmlingen R, Eberlein E, et al. Pushing the limits of in vivo diffusion MRI for the human connectome project. *Neuroimage* 2013; 80: 220–233.
13. Keil B, Blau JN, Biber S, et al. A 64-channel 3T array coil for accelerated brain MRI. *Magn Reson Med* 2013; 70: 248–258.1
14. Lian C, Zhang J, Liu M, et al. Multi-channel multi-scale fully convolutional network for 3D perivascular spaces segmentation in 7T MR images. *Med Image Anal* 2018; 46: 106–117.
15. Zhang H, Schneider T, Wheeler-Kingshott CA, et al. NODDI: practical in vivo neurite orientation dispersion and density imaging of the human brain. *Neuroimage* 2012; 61: 1000–1016.
16. Daducci A, Canales-Rodriguez EJ, Zhang H, et al. Accelerated microstructure imaging via convex optimization (AMICO) from diffusion MRI data. *Neuroimage* 2015; 105: 32–44.
17. Thomas C, Sadeghi N, Nayak A, et al. Impact of time-of-day on diffusivity measures of brain tissue derived from diffusion tensor imaging. *Neuroimage* 2018; 173: 25–34.
18. Gaberel T, Gakuba C, Goulay R, et al. Impaired glymphatic perfusion after strokes revealed by contrast-enhanced MRI: a new target for fibrinolysis? *Stroke* 2014; 45: 3092–3096.
19. Wardlaw JM. and William M. Feinberg award for excellence in clinical stroke: small vessel disease; a big problem, but fixable. *Stroke* 2018; 49: 1770–1775.
20. Patankar TF, Mitra D, Varma A, et al. Dilatation of the Virchow-Robin space is a sensitive indicator of cerebral microvascular disease: study in elderly patients with dementia. *AJNR Am J Neuroradiol* 2005; 26: 1512–1520.
21. Bouvy WH, van Veluw SJ, Kuijf HJ, S. Gov't, et al. Microbleeds colocalize with enlarged juxtacortical perivascular spaces in amnestic mild cognitive impairment and early Alzheimer's disease: a 7 tesla MRI study. *J Cereb Blood Flow Metab* 2020; 40: 739–746.
22. Goodman JR and Iliff JJ. Vasomotor influences on glymphatic-lymphatic coupling and solute trafficking in the central nervous system. *J Cereb Blood Flow Metab* 2020; 40: 1724–1734.
23. Zeppenfeld DM, Simon M, Haswell JD, et al. Association of perivascular localization of aquaporin-4 with cognition and Alzheimer disease in aging brains. *JAMA Neurol* 2017; 74: 91–99.
24. Benveniste H, Liu X, Koundal S, et al. The glymphatic system and waste clearance with brain aging: a review. *Gerontology* 2019; 65: 106–119.